Electrochimica Acta 427 (2022) 140793

Contents lists available at ScienceDirect

Electrochimica Acta

journal homepage: www.journals.elsevier.com/electrochimica-acta

Operando neutron imaging study of a commercial Li-ion battery at variable charge-discharge current densities

Nazia S. Nazer [a,b], Markus Strobl [c], Anders Kaestner [c], Preben J.S. Vie [a], Volodymyr A. Yartys [a,b,*]

[a] Institute for Energy Technology, Kjeller, Norway
[b] NTNU, Trondheim, Norway
[c] Paul Scherrer Institute (PSI), Switzerland

ARTICLE INFO

Keywords:
Operando neutron radiography
Neutron tomography
Li ion battery
Layered oxide cathode
Graphite anode

ABSTRACT

We report an *operando* neutron imaging study of a commercial ICR 10440 Li ion battery during charge and discharge. The cylindrical battery with a spiral configuration is composed of a multiphase layered oxide cathode and graphite anode. In spite of a two-dimensional nature of the projection data of this time-resolved study, structural and functional details of the neutron radiography study were successfully uncovered and visualized. The spatially resolved measurements with a resolution of 40 μm enabled to observe Li redistribution between the electrodes as well as a circulation of the electrolyte between the central column and the electrode layers at different states of charge (SoC) and at different current rates. Furthermore, *ex-situ* tomographic studies of the battery revealed the fine details of the structural inhomogeneity within the cell.

1. Introduction

In the emerging market of electric vehicles, high power batteries with improved cycle life are essential. Lithium ion batteries are recognized as an integral technology for serving the needs of energy supply. The use of lithium ion batteries in electric vehicles requires a life time exceeding 1000 cycles. To achieve this, a detailed study of the mechanisms of the battery performance is required. Many characterization techniques such as SEM, XRD, NMR provide insights into the occurring phenomena including electrodes cracking, particles fracture and surface films formation.

Internal structural transformations in the electrodes proceeding during charge-discharge influence the performance and lifetime of the batteries. These electrode structures are difficult to preserve when the metal housing of a battery has to be opened to analyse the interior. However, the battery interior can be visualized using neutrons thus enabling a non-destructive characterisation. The advantage of neutron imaging over the other imaging techniques is that neutrons interact with the nuclei of the constituent materials rather than with the electrons of the atoms. The signature property of the neutrons - their electrical neutrality - makes them highly penetrating into the structural materials. This allows the investigation of the interior of large objects and assemblies non-destructively. Furthermore, the application of neutron imaging to the lithium-ion batteries is very relevant when compared with X-ray imaging due to a high sensitivity of neutrons to the light elements in particular to hydrogen and lithium, because of a high absorption of neutrons by both these elements which enables direct observations of lithium redistribution, electrolyte consumption, and gas formation in lithium batteries [1]. Neutrons produce no radiation damage to the batteries, while beam damage with Synchrotron X-rays is sometimes at issue. The isotopic sensitivity offered by neutron techniques helps in the dynamic investigation of the materials evolution with extensive image contrast adaptability [1]. Hence, neutron imaging has been applied in the direct measurements of the Li ion transport in the batteries [2] based on a large neutron absorption cross-section of Li nucleus of 70 barn [3].

Several neutron imaging-based studies of Li ion batteries have been recently published [4–8]. 2D radiographic studies of the batteries have in general been limited to the specific simple geometries including custom built planar cells [9], which have been probed either in plane or in a through-plane geometries. The through plane geometry has a disadvantage of the fact that the thin layers when passed by the beam give a little contrast and thus the exchange reactions between the layers cannot be resolved. However, such phenomena as gas evolution can be studied [5,10]. In plane measurements face the difficulties of a relatively low spatial resolution of most neutron imaging systems of around 100

* Corresponding author at: Institute for Energy Technology, P.O. Box 40, Kjeller No 2027, Norway
E-mail address: volodymyr.yartys@ife.no (V.A. Yartys).

https://doi.org/10.1016/j.electacta.2022.140793
Received 5 April 2022; Received in revised form 7 June 2022; Accepted 1 July 2022
Available online 6 July 2022

μm, i.e. of the range of electrode layers thicknesses and interlayer distances. However, utilizing custom made systems with simplified layer structure proved that it is possible to probe interesting aspects of battery operation, including swelling [11] and Li exchange [12] between the layers during the cell operation. Problems like Li deposition on the anode during overcharging [7] and the consumption of excess electrolyte during the SEI formation [13] can also be analysed using neutron radiography studies.

For the cylindrical commercial cells, the 3D tomographic neutron imaging studies have been performed in [14–17], being focused on the studies of distribution of Li and electrolyte in the cells, including the data concerning generation and distribution of gas [5] in the cells. Despite the relatively slow rates used in the studied processes, the data on Li distribution/redistribution between the individual electrode layers was however beyond reach, particularly for the time resolved operando tomography studies. The data evaluation is limited by the low values of phase space density available from the neutron sources which is required for the good quality neutron imaging.

Similar limitations also appear for the neutron diffraction studies and in particular for the neutron imaging studies at so called Bragg edges, which exploit the contrast from diffraction interaction in the investigated materials. Specific custom designed geometries and cells and stroboscopic exposure are employed to challenge these limitations. Periodic stroboscopic diffraction [18] method was employed to achieve a good resolution during the neutron diffraction studies of the commercial cylindrical batteries [19]. Bragg edge analysis by 2D imaging was employed [4] to study the charge/discharge processes in a prismatic lithium-ion polymer battery [15]. The irreversible expansion of pouch cell correlating with capacity loss during the cycling was investigated by utilizing the stroboscopic neutron imaging technique [11]. 3D Bragg edge radiography was used for studying the crystallographic transitions in the cathode and anode of a commercial 18650 lithium ion battery [20] and mapping the lithium concentration at different state of charges.

Earlier performed neutron imaging studies on Li ion batteries showed a high potential for the use of neutron radiography to examine the Li redistribution process and electrode expansion [21]. Commercial primary Li ion cells were studied by neutron tomography to probe the Li diffusion/distribution processes [2,22]. High spatial resolution is required to achieve reasonable data on thin tailored electrodes that enables to study commercial Li-ion cells when at high charge-discharge currents. High resolution (20 μm) neutron radiography was utilized to investigate the lithium transport in a custom made $LiFePO_4$/graphite pouch cell [23] with electrodes thicknesses between 40 and 100 μm. Operando neutron radiography was used to demonstrate the particle evolution during the lithium alloying in Si anodes [24] by using an advantage of a decreased neutron transmission. High speed X-ray computed tomography and radiography was utilized to diagnose the thermal runaway in LG 18650 NMC cells [25] where structural degradation at high temperatures was observed.

In present study we demonstrate how a straightforward two-dimensional spatially resolved operando neutron imaging approach enables to perform time resolved high resolution studies of the commercial LIB cells and in particular to probe the redistribution of Li between the individual electrode layers. The radiography technique used in this study provides a better spatial as well as time resolution. Neutron tomography provides a complementary and more detailed data and allows the acquisition of images by rotating the sample in step wise manner. Then, the entire volume of a studied sample can be reconstructed in 3D visualisation from the collected projections.

The object of the presented study was a 360 mAh commercial cylindrical ICR 10440 lithium ion battery. This battery had earlier been studied by us using *operando* neutron diffraction and the results were published in [26]. The studied battery is composed of a multicomponent cathode containing a three-phase mixture of Li(Ni, Mn, Co)O_2, $LiCoO_2$ and $LiMn_2O_4$ and graphite as the anode electrode. The main objective of the study was in observing the exchange and redistribution of lithium between the individual anode and cathode layers as related to the state-of-charge/discharge of the cylindrical battery at different current rates when utilising the 2D nature of the radiographic projection measurements. Neutron tomography was furthermore utilized to study the mechanical changes in the commercial battery windings as a result of charging at high C-rates.

2. Experimental setup and data acquisition

The used commercial ICR 10440 cylindrical Li ion battery with a discharge capacity of 360 mAh had dimensions of 10 mm in diameter and a length of 40 mm. The cell contains alternating double sided current collectors - Al and Cu, a three-phase mixture of Li(Ni,Mn,Co)O_2, $LiCoO_2$ and $LiMn_2O_4$ as the cathode and graphite as the anode [26]. The electrodes are separated by a polymer membrane. The negative and positive electrode thickness is 136 μm (both sides) with 10 μm copper and aluminium foils backing. The separators are 20 μm thick. The battery consists of several layers in total formed by rolling of the double-sided electrodes and the separator layers.

The 10 mm diameter and the complicated multilayer winding design of the cylindrical battery restricts the usage of a broad range of analytical techniques for *in situ* characterization of the commercial battery to investigate the structural features and Li distribution changes during the operando studies.

Neutron Imaging has been performed at the ICON (Imaging with Cold Neutrons) [27] beamline at the continuous neutron spallation source SINQ of the Paul-Scherrer Institute (PSI), Switzerland. This beamline provides cold neutrons at a collimation ratio L/D = 343 (aperture D = 20 mm, source to sample distance L = 7 m), which defines the spatial resolution capability [28]; the beam at the sample position has a flux of 1.3×10^7 neutrons cm^{-2} s^{-1} mA^{-1}.

A ^{6}Li/ZnS scintillator with a thickness of 50 μm, optically coupled by a 45° mirror and light optics to a 2k*2k 16-bit Andor (DV436) CCD camera were used as the imaging detector. The field of view (FOV) was 82×82 mm^2 and corresponds to a pixel resolution of 40 μm.

One dark field (closed beam) and one flat field (open beam) image were collected prior to the collection of the sample data. The exposure time for the image collection was 20 s. All acquired images with the sample and the flat field image were first corrected for the background radiation by subtracting the dark field (DF) image. Subsequently the flat field correction was applied to the raw radiographs to remove artefacts by dividing by the open beam (flat field, FF) image. Fluctuation in the neutron flux from the source over time was corrected by normalizing all images by an average value of an open beam area, i.e. outside any sample material projection, within the same image. (Note that images were recorded against time, not a beam monitor. The open beam area in an image can replace a monitor count.) Image analysis software ImageJ [29] was used for processing the data and the collected time stamped radiographs were compiled into a movie.

During the *operando* study a periodic current profile was applied to the battery as shown in Fig. 1 and image acquisition was synchronized with the start of each cycle. Each image during the charge and discharge periods had an exposure time of 20 s while the images were acquired with 4 min intervals. Twenty-six images, with exposure time 20 s, were acquired during each charge and discharge period. Due to a source downtime during the 2nd charge at 1C and part of the discharge at 2C (143 t 258 min in Fig. 1) these images were not possible to collect.

During the neutron imaging experiments, the battery was connected to a BioLogic potentiostat. The battery was charged and discharged at 1C rate in the voltage window 3.0–4.2 V with an OCV period of 10 min in between. In the second cycle, the battery was cycled at 2C rate with an OCV period of 10 min after the 2 C discharge. An OCV period of 1 h was kept after the final 2C charged state. A CV cut-off C/10 was applied after the charging with no CV cut-off for the discharge.

The corresponding galvanostatic charge-discharge profile of the battery at 1C and 2C rate can be found in Fig. S1. The battery is first

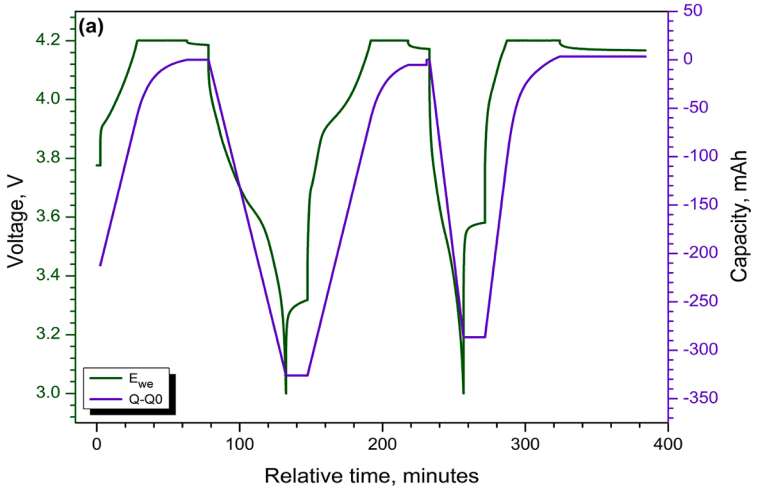

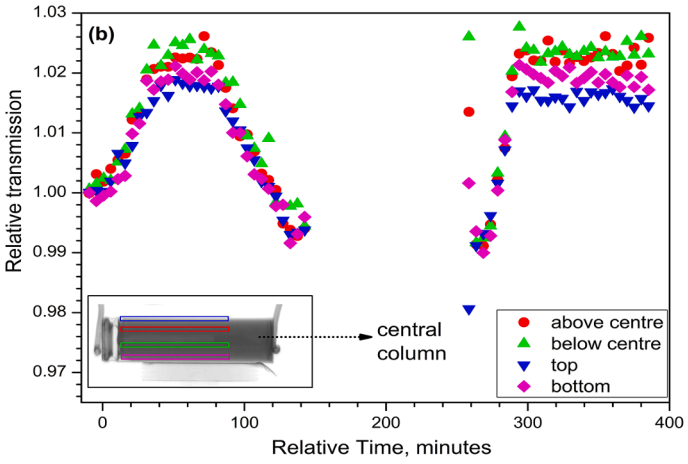

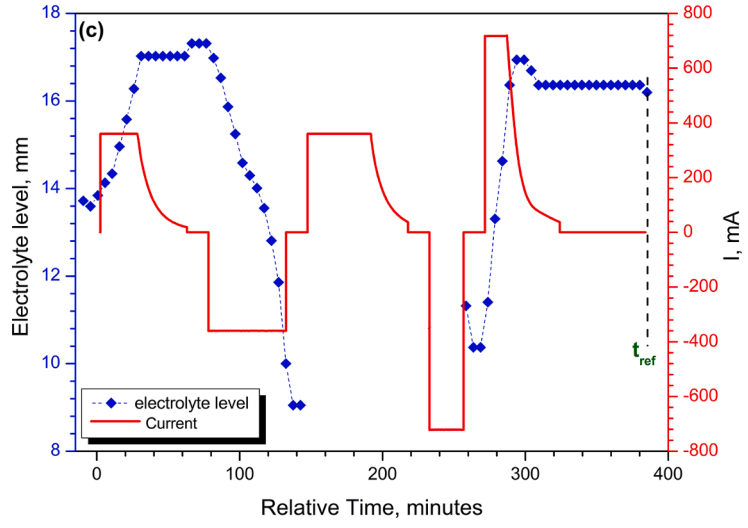

Fig. 1. (a) Galvanostatic voltage profile applied to the battery during the cycling; (b) Time dependent relative contrast for the selected pixel regions in the layered periphery (averaging regions marked in the inset) of the battery representing the corresponding uptake and reduction of electrolyte concentration; (c) Electrolyte level variation in the central column of the battery during in-situ charge-discharge at 1C and 2C rate. Note: After the fully discharged state at 1C, neutron beam was lost until the last stages of discharge at 2C. Hence some of the images are missing and correspondingly also the respective data points.

charged at 1C (360 mA) in the voltage range 3.0–4.2 V, from the initial discharged state as received from the manufacturer. At the applied testing conditions, the battery showed a discharge capacity of 326 mAh at 1C, which is about 90% of the rated capacity. With increase in current density, the discharge capacity is reduced to 286 mAh at 2C. During the charging the voltage limit is set to 4.2 V, which is the reason for a flat voltage profile at the end of the charge.

Tomography measurements of the same battery were performed for a fully charged at 2C battery. For the tomographic measurements, Gd-based scintillator with 20 μm thickness is used. A 300-projection data

set over 360° was acquired using a 1024*1024-pixel camera Andor NEO with a resolution of 27.8 μm. The tomograms were reconstructed using a large number of images taken at smaller angular increments with a total number of projections 300, using Tomviz software [30].

3. Results and discussions

3.1. Operando neutron radiography study

The cylindrical battery can be described as a stack formed by cathode, separator (pre-soaked in electrolyte), anode and another layer of separator placed on a top of one another, which is rolled into a kind of a Swiss roll type cell. When rolled together, a central hollow tube is formed which is partly filled with excess electrolyte.

The overall cylindrical shape implies a corresponding attenuation signature with a significantly increasing attenuation towards the center of the cylinder, which is typical for a relatively homogeneous attenuation throughout the cylinder. However, the hollow part of the central cylinder, which is not filled with electrolyte, displays an inverse contrast behavior, i.e., a little peak in this region (Fig. 2). The electrolyte provides significant contrast due to the high hydrogen content in the organic electrolyte solvent, having a relatively low Li volumetric concentration as compared to the electrodes. The single layers of the rolled battery structure around this central column are not resolved because they are covered up by the cylindrical geometry and its strong attenuation signature. Hence, in single radiographies at this stage only overall features like the filling state of the electrolyte, which is alternating during charge and discharge between the central column and the interlayered structure, can be observed straightforward.

The analysis of the neutron radiography data was performed by assuming that the observed neutron transmission/attenuation is related to the variations of the volumetric lithium content between the electrodes – anode and cathode, and electrolyte/soaked separator. We compared the changes in the attenuation of the neutrons by the electrodes by accounting the changes taking place during charge and discharge, and by the electrolyte after summing up a contribution from $LiPF_6$ and from hydrogen contained in the EC/DMC. Our calculations (see Supplementary Information file) showed that Li content in the electrolyte (1 M $LiPF_6$ solution) is 6.94 g Li/ 1000 mL. When adding up a contribution from hydrogen in EC/DMC, it appears to be equivalent to the overall Li content in the electrolyte solution of 9.33 g Li / 1000 mL. This is because the attenuation of neutrons by Li is 200 times higher than that for hydrogen. Thus, we focused on comparing the contribution from Li accommodated in the electrodes. When comparing the volumetric density of Li in the electrolyte and in the electrodes in the charged and discharged state, we observe that Li content in the electrodes appears to be 11-38 times higher than in the electrolyte/separator. Thus, we conclude that it is a change in the relative content of Li in the electrodes achieved via its redistribution during the charge-discharge process of the studied battery which has been monitored in the neutron radiography study performed in this work. For the electrolyte, the studied effect (including the contribution from H) appears to be relatively marginal.

Analyzing the filling height of the central column alone displays an obvious correspondence to the battery charge and discharge state (Fig. 1). The total length of the hollow central tube is 34 mm, of which about 14 mm is filled with the electrolyte in the initial state. Neutron radiographies of the battery charged/discharged at 1C and 2C show the reduction in the electrolyte level in the center hollow tube are provided in the Supplementary Information file, Fig. S2. During the charging process, the amount of excess electrolyte, which is mainly stored in the middle core of the battery, is increased. This is because during the charging the thickness of the graphite anode increases due to the volume expansion caused by lithium insertion and the electrolyte is forced out into the centre column of the battery (see Figs. 1c, S3 and Movie S1). The maximum expansion of the graphite anode is assumed to be around 12.7 %, which was calculated from our earlier diffraction study on this battery when LiC_6 was formed [26]. During the Li re-insertion into the cathode and a contraction of the anode, the excess electrolyte from the centre column of the battery is steadily accommodated by the electrodes (see Figs. 1c, S3 and Movie S1). When Li is reinserted back into the cathode, the volume changes are recovered, since the lithiated graphite contracts back to graphite, while the volume changes in the cathode layered oxides are very small as related to the state of their lithiation, which causes the electrolyte to circulate back into the porous electrode layers. This excess electrolyte helps to maintain the Li-ion conductivity between the electrodes during operation. When compared with the fully charged state at 1C, the excess electrolyte level in the centre column is reduced after the 2C charge (Fig. 1(c)). This implies about 7.7% reduction of the electrolyte level in the centre column during the cycling of the battery. Averaging over different radial regions mirrors the same behavior, but is inverse to the central column, underlining the exchange

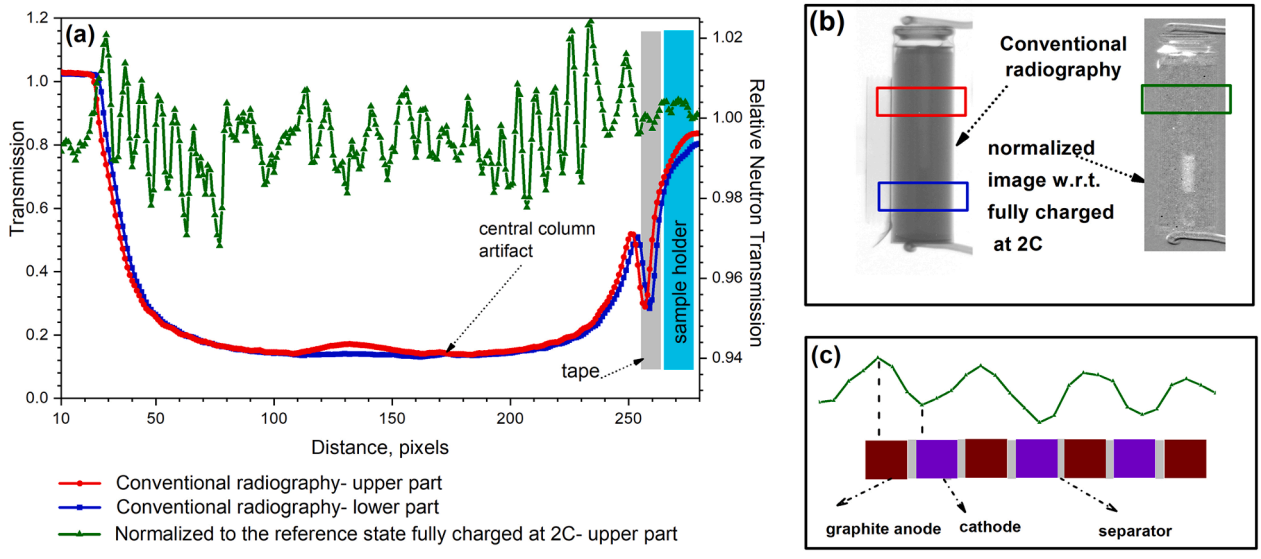

Fig. 2. (a) Comparison of the line profiles at different heights of the battery from conventional radiographic images with a line profile of an image at discharged state normalized with the final image at full charge; (b) Corresponding images and locations of line profiles; (c) Details of line profile in (a) from the image normalized with respect to the final state and the schematic correspondence of the projection of the layered cell structure.

of electrolyte between the center and the periphery. A similar change in the electrolyte level was observed in a Li/MnO_2 primary battery [2] during the discharge process studied by neutron tomography.

In order to further extract structural information, in particular to assess the Li redistribution during the charge and discharge, the recorded images have to be normalized by a reference state. Such normalization levels out the cylindrical footprint and highlights only changes between the reference state and any other state. Due to the fact that the biggest change during the charge and discharge, besides the electrolyte level, is the redistribution of Li between the electrodes, while the rest of the structure remains largely unaltered on the probed length scale (resolution of about 80 micrometers), we will demonstrate that this redistribution can be evaluated.

Hence, for the further analyses radiographic images are normalized with respect to a reference image mostly to the final image collected at a relaxed state (after a completion of the resting period following the battery charge at 2C). In such a way the relative change in lithium distribution becomes visible (Fig. 2a). Despite the cylindrical geometry and the 2D nature of the radiographs (Fig. S2) the normalization by the reference image reveals significant details of the internal structure of the battery and Li migration (Fig. 2c). Due to the change in Li distribution, the individual layers can be resolved, in particular in the charged/discharged states of the battery opposed to the one of the reference images. Fig. 2a displays the effect of the normalisation and how the observed fringes correlate with the structure of the battery (Fig. 2c).

Consequently, this data normalisation allows for the first time a detailed study of the process and different stages of charge and discharge with spatial resolution, focussing on different areas of the battery and individual layers. The effect, which is just of the order of percent in the transmission image, governs the images as relative to a reference state as

$$I_{ref} = \frac{I}{I_{ref}} I_0 e^{-(\mu_s t_s + \mu_e t_e + \mu_{Li} t_{Li})} \Big/ I_0 e^{-\left(\mu_s t^{ref}{}_s + \mu_e t^{ref}{}_e + \mu_{Li} t^{ref}{}_{Li}\right)} = e^{-(\mu_s \Delta t_s + \mu_e \Delta t_e + \mu_{Li} \Delta t_{Li})}$$

where $\mu_s t_s$ is the attenuation of the overall structural elements with attenuation coefficient μ_s and thickness t_s in the battery, which can largely be assumed not to change during the process so that $\mu_s \Delta t_s = 0$ and the images relative to the reference only display contributions of change in electrolyte content Δt_e and Li distribution Δt_{Li}. These can be distinguished due to the fact that the electrolyte affects all individual layers while Li migrates between the cathode and anode electrodes. Hence, the electrolyte influx or expulsion from the layered structure can be observed as an increase or decrease, respectively, of the offset of the observed curves and in particular the modulation pattern which represents the redistribution of Li between the electrodes. Therefore, the contributions of Δt_s, Δt_e and Δt_{Li} can largely be separated. However, the cylindrical shape of the layered structure poses some limits on the resolution of Li redistribution between individual electrode layers, as in the projection images, different orientations and individual layers are superposed. Nevertheless, the data reveals that for the outer part, about 2/3 of the layers, the Li redistribution between the layers and hence the individual electrodes and their Li exchange can be resolved (compare Fig. 2a). This provides a rich qualitative information about the process and local differences, while at this stage a precise quantification of the Li redistribution is hindered because of a lack of the sufficient amount of data, and further measurements and simulations need to be performed.

Fig. 3. (a–d) shows the line profile comparison of the battery at fully charged and discharged states at 1C and 2C, in the marked region (e). Fig. 3a demonstrates that the structure of the layers did not alter in the given area during the charge/discharge processes at different C rates, as there is no change in the corresponding fringes position. Even their relative behaviour, i.e. the ratio between the subsequent maxima seems unaltered in the final discharged state. As the position of the fringes does not change, independent of the state of the battery – charged/discharged, and independent of the current densities applied during the experiments – 1C or 2C, we conclude that the battery architecture gives the electrode enough flexibility to accommodate a marginal maximum expansion of the battery anode – 5–8 μm (which is far below a level of resolution of the neutron radiography images available in the present study). This however does not affect the macroscopic architecture of the battery and the relative positions of the battery layers remain unchanged. However, the offset of the intensity modulation, which can be attributed to a significant contribution of the change in Δt_e well agreed with the findings of the initial investigation of the electrolyte redistribution during charge and discharge. It can be seen from Fig. 3c and d, that the mean neutron transmission is lower at the electrode windings in the fully discharged states, due to the highest volumetric concentration on Li in the layered oxide cathode (as compared to anode and electrolyte) which becomes saturated by Li. Furthermore, the amount of

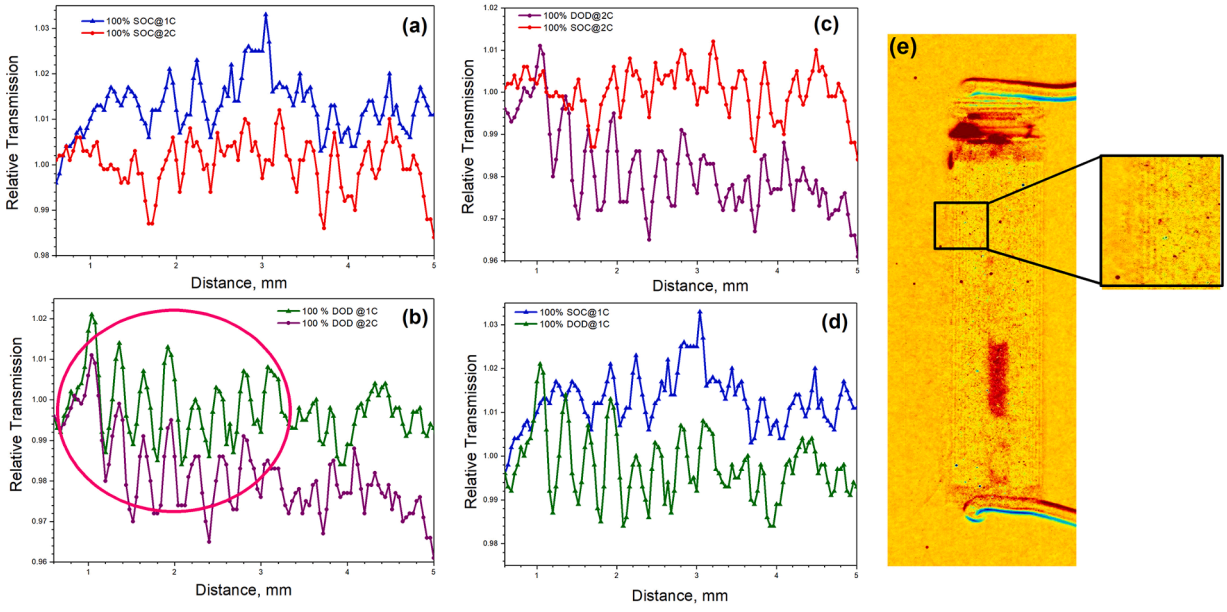

Fig. 3. (a) Comparison of fully charged states at 1C and 2C; (b) Comparison of fully discharged states at 1C and 2C; (c) Comparison of fully charged and fully discharged states at 2C; (d) Comparison of fully charged and fully discharged states at 1C; (e) Radiographic image of the discharged battery normalized to fully charged state and details of the area vertically averaged and depicted in (a–d).

electrolyte in the electrodes, separator and a buffer volume changes as related to the applied current density, 1C or 2C, as is evident from the Fig. 3b.

In Fig. 4 the axial top, middle and bottom parts (as marked in Fig. 4d) of the battery are compared at the fully discharged state at higher current rate. Fig. 4 (a–c) shows a comparison of the left side of the battery which underlines that neither the structure nor the process is completely homogeneous over the axial part of the battery. The blue plot in Fig. 4(e) shows the neutron transmission profile in the marked region of the right side of the battery at 100% DOD at 2 C rate and the data shows the difference in neutron transmission throughout the battery. Differences can be observed in the relative electrolyte content as well as Li exchange between the individual layers at different heights of the cell. It can be seen from Fig. 4 (e–g) that the Li distribution process is significantly heterogenous over the axial part of the battery on the right side also. On the other hand, on the radial axis, the Li distribution is symmetrical at both sides of the battery near both current collectors, whereas the Li distribution at the middle part of the discharged cell is asymmetrical. The periodicity of the transmission profile is repetitive near the bottom part, as seen in Fig. 4g, which shows the structural homogeneity at this region. Also, a very similar Li distribution was found between the totally discharged state at 1C and 2C. However, this comparison looks quite different in Fig. 4f, where the similarity of these states is disturbed by significant differences for the third layer repetition (marked in yellow). It appears that for the discharged state at 1C either a structural variation or emergence of defects occur, or the Li exchange between the electrodes is disturbed / hindered in this position between the individual electrodes at that specific height. The behaviour at 2C however appears to be more normal, which is why the appearance of general structural defects is unlikely. However, it has to be noted that in general the redistribution and hence the functionality of the battery at this specific height does not appear as regular as in other positions, which might be a signature of some structural irregularity / inhomogeneity. The relaxation time of 1 h applied after the fully discharged state at 2C was also monitored to analyse the change in Li gradient between the electrode layers during the resting time. As can be seen from Fig. 4e, there is a significant change in the Li relaxation rate after 45 min of OCV period and 50 min of OCV period. This implies that a time-dependent redistribution of Li in the electrodes takes place via its diffusion, further to the fact that the electrolyte flow into the electrode layers continues with some time delay even without applied current, which can also be observed by the change in the excess electrolyte amount in the middle core of the battery (see Supplementary file, movie S1).

While the normalisation to the final state, which is fully charged battery at 2C, enables to observe only the differences with regards to this state, a normalisation with e.g. the initial image changes this situation. By focusing on the discharge process at 1C, a comparison is made between normalising the images with reference to the fully charged state at 2C and the initial state (which corresponds to about 1/3rd of the fully charged state at 1C), at different depth of discharge (DOD) as shown in Fig. 5. In the normalisation against the fully charged state at 2C, the 25% discharged at 1C state displays no fringe pattern, but only the difference in the electrolyte filling between the two states, which implies a very similar Li distribution at these two states (Fig. 5a). During the discharge process, Li from the graphite anode is mostly removed, which is detectable by the intensity increase in the electrode, from the radiograph transmission line profiles. The more the battery is discharged at 1C, the more the modulation pattern grows and gains a regular shape (Fig. 5b–d) culminating in a very regular and well-known fringe structure in Fig. 5d. In contrast, this comparison looks very different in Fig. 5f-i, where the same images are normalized with the initial state at 1C. In Fig. 5i, the fully charged state and initial state at 1C are compared and display a fringe pattern which is shifted by half a period, as one image depicts the movement of Li to the anode and the other to the cathode. The fringes in these curves are less pronounced, obviously because the reference image is closer to the depicted states than in the other curves comparing fully charged and discharged states with respect to a fully charged image. The distortion observed in these patterns however reveals another detail. The outer and inner layers of this region in the battery appears to experience different fraction of Li exchanges between cathode and anode at different times of the process, i.e. at different overall charging states. The difference in Li distribution to the initial state for the outer layers differs the most for the reference at 25% discharge (Fig. 5f) while the innermost resolved layers differ most significantly at 75% and at full discharge (Fig. 5h, i). At 50% (Fig. 5g) the differences appear at a minimum. As the development is however

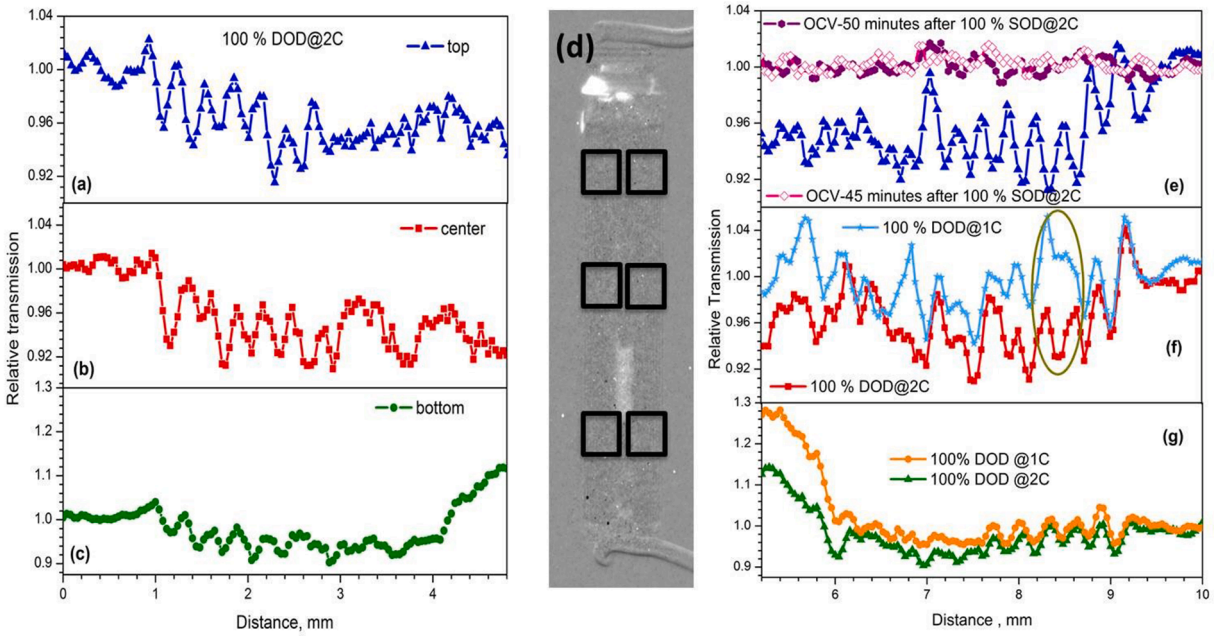

Fig. 4. Comparison of discharged state (at 2C) as normalized to final fully charged state at different areas of the battery cell; (a–c) Left side of the battery at different heights as indicated in (d); (e–g) Right side of the battery at different heights as indicated in (d) Compared to fully charged state in (e); Compared to fully discharged state at 1C in (f) & (g).

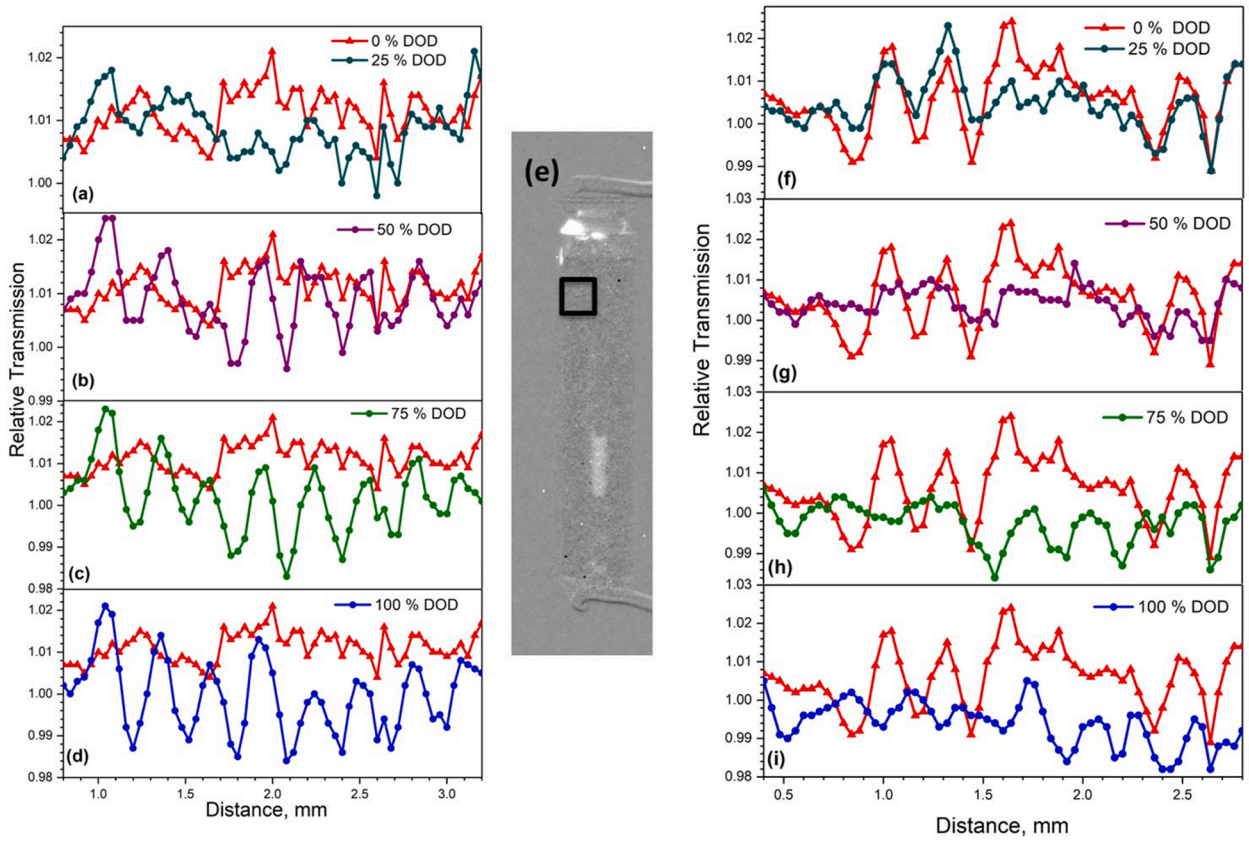

Fig. 5. Different states of discharge at 1C compared to the fully charged state (0% DOD) as referenced to the fully charged state at 2C (a–d) and referenced to the initial state of the battery (app. 1/3 charged) (f–i) at the position indicated in (e).

homogeneous in the left column of the Fig. 5(a–d) with regards to the reference at the well-known final state, it can be concluded that in the initial state of the battery taken as reference for the right column (f–i) the charging state, i.e. distribution of Li between anode and cathode, is not homogeneous with respect to the layers. The layers in the initial state are at different individual charging states, i.e. the cell was initially more charged in the inner layers than in the outer layers.

When normalizing the states of discharge at 1C with the respective previous state in steps of 25% of discharge (shown in Fig. S4), a differential change during the process is visualized. As differences are however relatively small in such normalization, the curves display relatively low signal and significant statistical variations in comparison. However, it appears again that Li exchange is first more significant in the outermost layers and is delayed in the central layers. While the electrolyte uptake in the outer layers seems to be smooth and continuous, but smaller during discharge in the outermost layers, it appears that the process is delayed in consecutive layers towards the centre. This underlines the findings with regards to the previous Fig., while it is also shown in Fig. S4 b, referencing the fully discharged state at 1C to the fully charged battery at 1C and 2C, respectively, there are produced very similar exchange patterns. The neutron transmission at 100% SOC (fully lithiated state of graphite) is reduced due to the increased Li concentration after the charge is completed. These differ mainly with respect to the specific amplitudes and offsets, which can be expected as discussed earlier for the different charging/discharging conditions. Furthermore, no gas evolution was observed in either study as reported in the literature for the conditions departing from a normal battery operation [2,25,31].

3.2. *Ex situ neutron tomography study*

The orthogonal tomographic slices of the fully discharged at 2C battery at different heights of the battery are shown in Fig. 6 (ii). The Swiss roll construction is clearly visible. At the core of the cell, a hollow region is visible, which is highly attenuating due to the presence of lithium-containing electrolyte and there is no cylindrical support to aid the cell winding to give mechanical support. The outer steel casing of the battery remains intact along the battery height. The tightly wound electrode, current collector and separator layers remain intact at the negative side of the battery. However, a small degree of delamination was observed near the outer diameter of the battery where the spiral–wound layers are the least compressed. Structural deformation around the inner and outer layers was observed near the positive side of the battery. The very bright region (golden colour) along the outer circle of the battery is the Al current collector. It is clear that the outer layer is deformed when we move along the axial direction to the positive electrode region. This divergence between the layers could be aimed to provide space for the accommodation of local gas generated from the processes such as electrolyte degradation and SEI layer breakdown [25]. The dark core region (navy blue colour) is the centre hollow column formed by the separator winding. It is filled with electrolyte in the lower part of the battery. As going up along the axis, diameter of the core region increases and scatters less showing bright spots. This is due to the decreased electrolyte volume. The scattering varies along the radial direction of the battery due to the difference in Li concentration. 3D visualization of the studied Li-ion cell (fully charged), reconstructed from the tomographic slices acquired with a total of 300 projections with 90 s exposure time is shown in Fig. 6 (iii).

Tomography of the cell provided cross sectional images of the battery and evidence for the structural inhomogeneity within the cell. No central cylindrical support is present in the cell, which showed the structural distortion of the battery architecture on both the outer and inner regions close to the positive side of the battery. This explains the reason for the inhomogeneous Li distribution in the lower and upper

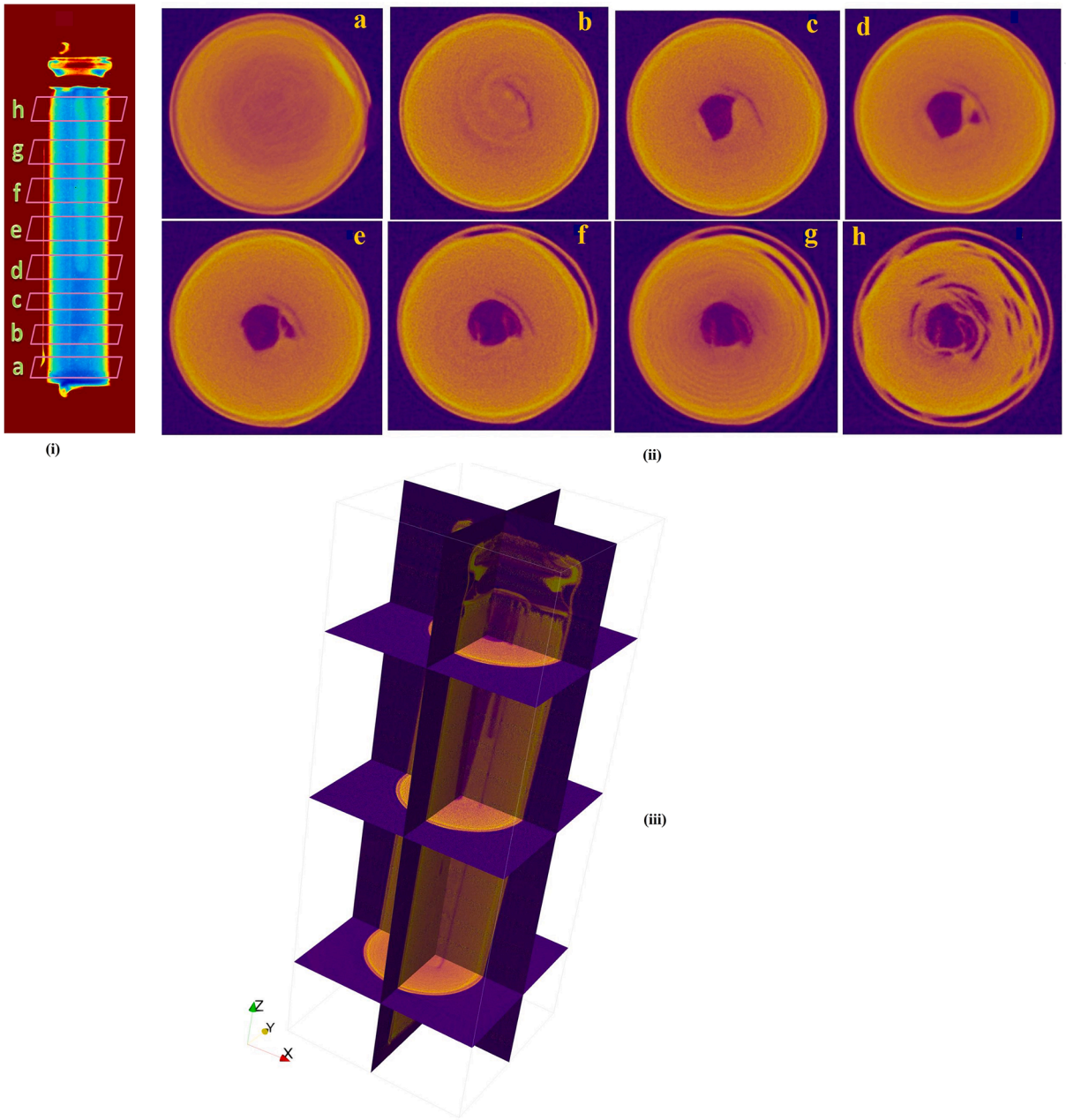

Fig. 6. Tomography slices from 3D reconstructions (ii) at different heights of the battery marked in the radiograph (i) and (iii) 3D visualization of the commercial ICR 10440 Li-ion cell (fully charged), reconstructed from the tomographic slices acquired with a total of 300 projections with 90 s exposure time.

regions of the battery along the axial direction. The inhomogeneous scattering of the battery slices along the radial axis confirms the non-uniform Li distribution across the battery at different charging states. This structural inhomogeneity can be avoided by including an internal structural support [14] in the battery design. In the X-ray tomography study of the 18650 NMC battery [25] without an internal support, structural collapse of the spiral wound electrode layers was observed during the thermal runaway studies. This collapse induced structural deformation in the battery layers which further increased the risk of severe internal short circuits and consequent thermal runaway. Such a collapse has not been observed in the cell with an internal support studied by the same group. Thus, tomography studies can be used as an effective tool to visualize the internal structure of the battery.

4. Conclusions

In this study operando neutron radiography has proven to be able to reveal a rich variety of information about the charge and discharge of a commercial LIB cell. Despite the cylindrical geometry, the exchange of Li between the electrodes can be depicted and qualitatively analysed for a large fraction of the battery. These insights allow addressing individual layers and providing local assessments of the performance and structure with respect to the Li exchange. Additionally, the distribution and re-distribution of electrolyte throughout the cell can be assessed and analysed.

The possibility of normalizing the images within a time series to different stages of the process provides detailed information about relative changes and hence exchange processes. The contrast is significantly enhanced for the changes in distribution and structure as compared to a conventional individual image, where many details are

buried because of the strong overall attenuation. Only the suppression of constant features of the unaltered structure during the process enables to reveal the desired details of the Li exchange reaction with full spatial resolution and hence with local relevance. Individual locations of alterations in the process can be identified.

The major features learned during the operando galvanostatic study of the battery at 1C and 2C of the battery with neutron radiography include:

Neutron radiograph study of the Graphite/mixed NMC oxide battery showed that neutron transmission has a peak (graphite anode) and valley (NMC cathode) periodical pattern which corresponds to the layers of the rolled battery architecture with several layers in the battery.

Further to the highly attenuating neutron elements, lithium, cobalt and hydrogen, causing neutron attenuation by anode, cathode and electrolyte, high porosity of both electrodes leads to the penetration of Li-containing electrolyte into the electrodes and further contributes to the absorption resulting in the corresponding changes in the overall neutron transmission. Particularly significant contribution to this feature is coming from the "breathing" of graphite anode which experiences expansion by appr. 12 % on lithiation to form LiC_6 followed by a less significant contraction on electrode discharge as lithium partially remains in non-decomposed LiC_{12}.

With the total electrode thickness of 136 μm assumes that graphite anode has a thickness of 70 μm, this 12 % expansion should result in a maximum increase in the thickness of the anode to 78 μm. We note that the expansion of 8 μm is probably overestimated as the electrode contains pores and the maximum achievable crystallographic expansion of 8 μm in reality will be lower. The resolution of the collected data from neutron radiography and neutron tomography is 40 μm and 27.8 μm, respectively, while the effect of be monitored expansion should be in the range 5–8 μm. Thus, a comparison of a real macroscopic expansion and the accuracy of the collected neutron imaging data concludes that it is not possible to resolve the real expansion with the given resolution. Nevertheless, the periodicity of the fringes appears to be constant while the distance between the fringes fits the interlayer dimensions in the battery as seen in Fig. 3 and is constant, independent of the state of the battery (charged/discharged) and a rate of the electrochemical processes – 1C or 2C. These distances are too large to cause any modulations during the cycling as the design of the battery interior can easily accommodate a marginal expansion occurring in the anode.

The central column of the battery works as a buffer volume where the level of electrolyte changes following charge/discharge of the battery. Expansion of graphite anode on charging leads to the expulsion of the electrolyte from the porous anode. The extent of electrolyte expulsion to the battery core is higher at the lower applied current density resulting from a more pronounced lithiation of the anode. Indeed, as the charge/discharge capacity decreases following an increase in current densities (probed at 1 C and at 2C, with charge/discharge capacities of 325/320 and 289/286 mAh, correspondingly), the extent of transformations in the anode on its lithiation-delithiation varies in the same way which causes the observed increase/decrease in the level of electrolyte.

The discharge capacity loss was 10.6% with current density increasing from 1C to 2C. At increased C rate, the amount of electrolyte expelled back to the central column was smaller. However, the most significant effect on the neutron transmission causes a change in the content of Li in the electrodes, as a part of the anode instead of converting to LiC_{12} remains in undischarged state as LiC_6 which causes a reduced neutron transmission for the 2C sample. This is clearly seen by examining the neutron transmission across the cell for the highest current density studied.

At the beginning of the discharge process, the distribution of intercalated lithium within the cathode is inhomogeneous throughout the battery layers. As the discharge continues, with more lithium re-intercalating into the cathode as observed in our previous neutron diffraction studies, Li distribution becomes more even and shows a homogeneous distribution along the radial axis of the battery. Possible read on for that is in a more even Li distribution between the particles of three individual cathode constituents - NMC and $LiCoO_2$ layered oxides together with $LiMn_2O_4$ spinel.

In the anode layers, Li distribution is inhomogeneous during the charge process, mainly due to the staged intercalation of Li into graphite to form LiC_6 via formation of LiC_{18} and LiC_{12} as observed in our earlier performed operando neutron diffraction studies [26]. Nevertheless, this will affect the macroscopic picture monitored by neutron radiography only by the changes of the gradual overall average lithium content in the studied anode electrode.

The structural and Li distribution inhomogeneity along the axial part of the battery observed from the radiography profiles is due to the variations of the lithium content between the electrodes as related to the state of the battery charge/discharge and current density employed to perform the battery cycling while the battery architecture within the cell remain unaltered independent of the applied electrochemical conditions.

In order to optimize the electrochemical processes in the commercial lithium battery cells by reducing the amount of active material in the cells, to reduce the costs and to achieve improved cell performance and capacity, it is important to study dynamic processes in such batteries operando. The elucidation of internal structure features has highlighted the effect of battery design on the behaviour of the cells.

In summary, operando neutron radiography and neutron tomography were used to directly assess the battery interior including battery electrodes and a distribution of the electrolyte during charge-discharge at two different current densities, 1C and 2C. The experiments showed an inhomogeneous lithium distribution, with more pronounced transformations occurring in the inner electrode windings with increased current rates. This indicates a more complete electrochemical process taking place in the inner cell sections.

The advantages of a 2D radiographic study lies mainly in a sufficient time resolution achieved, which with currently available experimental setups available at the leading neutron imaging facilities, including PSI, enables even a better spatial resolution and measurement accuracy than in the current pilot study.

Disadvantages of a limited quantification can still be overcome by a potential modelling based on the high resolution tomographies at stationary conditions and corresponding simulations and fitting. In addition, the approach of normalisation between the different states of charge and discharge could be applied for the tomographic 3D studies at selected stationary conditions.

CRediT authorship contribution statement

Nazia S. Nazer: Methodology, Investigation, Formal analysis, Data curation, Visualization. **Markus Strobl:** Methodology, Formal analysis, Visualization. **Anders Kaestner:** Investigation, Formal analysis, Visualization. **Preben J.S. Vie:** Investigation, Methodology, Data curation. **Volodymyr A. Yartys:** Supervision, Methodology, Funding acquisition.

Declaration of Competing Interest

The authors declare that they have no known competing financial interests or personal relationships that could have appeared to influence the work reported in this paper.

Data availability

Data will be made available on request.

Acknowledgment

This work was supported by Research Council of Norway and the European Spallation Source. The work is partly based on the

experiments performed at the Swiss spallation neutron source SINQ, Paul Scherrer Institute, Villigen, Switzerland. We sincerely appreciate help from ICON instrument responsible scientist Dr. David Mannes during the performed experiment # 20160934 “Tomographic Studies of Lithium-Ion Batteries – Kinetics and Failure Modes”. We are grateful to the marketing department of Great Power Battery Co., Ltd. (H.K./China) for sharing an overview of the technology development in the company, for providing the catalogue of the commercial products and for the battery cells utilized in the present study.

Supplementary materials

Supplementary material associated with this article can be found, in the online version, at doi:10.1016/j.electacta.2022.140793.

References

[1] R.F. Ziesche, N. Kardjilov, W. Kockelmann, D.J.L. Brett, P.R. Shearing, Neutron imaging of lithium batteries, Joule 6 (2022) 35–52.
[2] R.F. Ziesche, T. Arlt, D.P. Finegan, T.M.M. Heenan, A. Tengattini, D. Baum, N. Kardjilov, H. Markotter, I. Manke, W. Kockelmann, D.J.L. Brett, P.R. Shearing, 4D imaging of lithium-batteries using correlative neutron and X-ray tomography with a virtual unrolling technique, Nat. Commun. 11 (2020) 777.
[3] M. Eil, F. Kappeler, M. Wiescher, A. Mengoni, The (n, ϒ) cross section of ^{7}Li, Astrophys. J. 507 (1998) 997–1002.
[4] K. Kino, M. Yonemura, Y. Ishikawa, T. Kamiyama, Two-dimensional imaging of charge/discharge by Bragg edge analysis of electrode materials for pulsed neutron-beam transmission spectra of a Li-ion battery, Solid State Ionics 288 (2016) 257–261.
[5] B. Michalak, H. Sommer, D. Mannes, A. Kaestner, T. Brezesinski, J. Janek, Gas evolution in operating lithium-ion batteries studied *in situ* by neutron imaging, Sci. Rep. 5 (2015) 15627.
[6] T. Knoche, V. Zinth, M. Schulz, J. Schnell, R. Gilles, G. Reinhart, *In situ* visualization of the electrolyte solvent filling process by neutron radiography, J. Power Sources 331 (2016) 267–276.
[7] A. Same, V. Battaglia, H.Y. Tang, J.W. Park, *In situ* neutron radiography analysis of graphite/NCA lithium-ion battery during overcharge, J. Appl. Electrochem. 42 (2011) 1–9.
[8] D. Goers, M. Holzapfel, W. Scheifele, E. Lehmann, P. Vontobel, P. Novák, *In situ* neutron radiography of lithium-ion batteries: the gas evolution on graphite electrodes during the charging, J. Power Sources 130 (2004) 221–226.
[9] J.B. Siegel, X. Lin, A.G. Stefanopoulou, D.S. Hussey, D.L. Jacobson, D. Gorsich, Neutron imaging of lithium concentration in LFP pouch cell battery, J. Electrochem. Soc. 158 (2011) A523.
[10] B. Michalak, B.B. Berkes, H. Sommer, T. Bergfeldt, T. Brezesinski, J. Janek, Gas evolution in $LiNi_{0.5}Mn_{1.5}O_4$/graphite cells studied in operando by a combination of differential electrochemical mass spectrometry, neutron imaging, and pressure measurements, Anal. Chem. 88 (2016) 2877–2883.
[11] J.B. Siegel, A.G. Stefanopoulou, P. Hagans, Y. Ding, D. Gorsich, Expansion of lithium ion pouch cell batteries: observations from neutron imaging, J. Electrochem. Soc. 160 (2013) A1031–A1038.
[12] J.B. Siegel, X. Lin, A. Stefanopoulou, On the accuracy and simplifications of battery models using *in situ* measurements of lithium concentration in operational cells, in: Proceedings of the American Control Conference IEEE Conference, Montréal, Canada, 2012, pp. 1362–1367. Publications, Fairmont Queen Elizabeth.
[13] M. Lanz, E. Lehmann, R. Imhof, I. Exnar, P. Nova’k, *In situ* neutron radiography of lithium-ion batteries during charge/discharge cycling, J. Power Sources 101 (2001) 177–181.
[14] L.G. Butler, E.H. Lehmann, B. Schillinger, Neutron radiography, tomography, and diffraction of commercial lithium-ion polymer batteries, Phys. Procedia 43 (2013) 331–336.
[15] L.G. Butler, B. Schillinger, K. Ham, T.A. Dobbins, P. Liu, J.J. Vajo, Neutron imaging of a commercial Li-ion battery during discharge: application of monochromatic imaging and polychromatic dynamic tomography, Nucl. Instrum. Methods A 651 (2011) 320–328.
[16] A. Senyshyn, M.J. Mühlbauer, O. Dolotko, M. Hofmann, T. Pirling, H. Ehrenberg, Spatially resolved in operando neutron scattering studies on Li-ion batteries, J. Power Sources 245 (2014) 678–683.
[17] A. Senyshyn, M.J. Mühlbauer, K. Nikolowski, T. Pirling, H. Ehrenberg, In-operando” neutron scattering studies on Li-ion batteries, J. Power Sources 203 (2012) 126–129.
[18] M. Iizumi, Real-time neutron-diffraction studies of phase-transition kinetics, Phys. B & C 136 (1986) 36–41.
[19] X.L. Wang, K. An, L. Cai, Z. Feng, S.E. Nagler, C. Daniel, K.J. Rhodes, A.D. Stoica, H.D. Skorpenske, C. Liang, W. Zhang, J. Kim, Y. Qi, S.J. Harris, Visualizing the chemistry and structure dynamics in lithium-ion batteries by *in-situ* neutron diffraction, Sci. Rep. 2 (2012) 747.
[20] K. Kino, M. Yonemura, Y. Kiyanagi, Y. Ishikawa, J.D. Parker, T. Tanimori, T. Kamiyama, First imaging experiment of a lithium ion battery by a pulsed neutron beam at J-PARC/MLF/BL09, Phys. Procedia 69 (2015) 612–618.
[21] H. Zhou, K. An, S. Allu, S. Pannala, J. Li, H.Z. Bilheux, S.K. Martha, J. Nanda, Probing multiscale transport and inhomogeneity in a lithium-ion pouch cell using *in situ* neutron methods, ACS Energy Letters 1 (2016) 981–986.
[22] Y. Zhang, K.S.R. Chandran, H.Z. Bilheux, Imaging of the Li spatial distribution within V_2O_5 cathode in a coin cell by neutron computed tomography, J. Power Sources 376 (2018) 125–130.
[23] J.B. Siegel, A.G. Stefanopoulou, P. Hagans, Y. Ding, D. Gorsich, Expansion of lithium ion pouch cell batteries: observations from neutron imaging, J. Electrochem. Soc. 160 (2013) A1031–A1038.
[24] F. Sun, H. Markötter, I. Manke, A. Hilger, S.S. Alrwashdeh, N. Kardjilov, J. Banhart, Complementary X-ray and neutron radiography study of the initial lithiation process in lithium-ion batteries containing silicon electrodes, Appl. Surf. Sci. 399 (2017) 359–366.
[25] D.P. Finegan, M. Scheel, J.B. Robinson, B. Tjaden, I. Hunt, T.J. Mason, J. Millichamp, M. Di Michiel, G.J. Offer, G. Hinds, D.J.L. Brett, P.R. Shearing, In-operando high-speed tomography of lithium-ion batteries during thermal runaway, Nat. Commun. 6 (2015) 6924.
[26] N.S. Nazer, V.A. Yartys, T. Azib, M. Latroche, F. Cuevas, S. Forseth, P.J.S. Vie, R. V. Denys, M.H. Sørby, B.C. Hauback, L. Arnberg, P.F. Henry, In operando neutron diffraction study of a commercial graphite/(Ni, Mn, Co) oxide-based multi-component lithium ion battery, J. Power Sources 326 (2016) 93–103.
[27] A.P. Kaestner, S. Hartmann, G. Kühne, G. Frei, C. Grünzweig, L. Josic, F. Schmid, E. H. Lehmann, The ICON beamline – a facility for cold neutron imaging at SINQ, Nucl. Instrum. Methods Phys. Res. 659 (2011) 387–393.
[28] M. Strobl, I. Manke, N. Kardjilov, A. Hilger, M. Dawson, J. Banhart, Topical review: advances in neutron radiography and tomography, J. Phys. D Appl. Phys. 42 (2009) 243001–243022.
[29] J. Schindelin, I. Arganda-Carreras, E. Frise, V. Kaynig, M. Longair, T. Pietzsch, S. Preibisch, C. Rueden, S. Saalfeld, B. Schmid, J.Y. Tinevez, D.J. White, V. Hartenstein, K. Eliceiri, P. Tomancak, A. Cardona, Fiji: an open-source platform for biological-image analysis, Nat. Meth. 9 (2012) 676–682.
[30] B.D.A. Levin, Y. Jiang, E. Padgett, S. Waldon, C. Quammen, C. Harris, U. Ayachit, M. Hanwell, P. Ercius, D.A. Muller, R. Hovden, Tutorial on the visualization of volumetric data using tomviz, Microscopy Today 26 (2018) 12–17.
[31] G.A. Elia, G. Greco, P.H. Kamm, F. García-Moreno, S. Raoux, R. Hahn, Simultaneous X-ray diffraction and tomography operando investigation of aluminum/graphite batteries, Adv. Funct. Mater. 30 (2020), 2003913.